Journal of the Korean Electrochemical Society
Vol. 9, No. 1, 2006, 10-18

An Overview of the Activated Carbon Fibers for Electrochemical Applications

Gyoung-Ja Lee and Su-Il Pyun†

Department of Materials Science and Engineering, Korea Advanced Institute of Science and Technology, #373-1 Guseong-dong, Yuseong-gu, Daejeon 305-701, Republic of Korea

(Received December 30, 2005 : Accepted February 14, 2006)

Abstract: This article is concerned with the overview of the activated carbon fibers. Firstly, this review provides a comprehensive survey of the overall processes for the synthesis of the activated carbon fibers from the carbonaceous materials. Subsequently, the physicochemical properties such as pore structures and surface oxygen functional groups of the activated carbon fibers were discussed in detail. Finally, as electrochemical applications of the activated carbon fibers to electrode materials for electric double-layer capacitor (EDLC), the electrochemical characteristics of the activated carbon fiber electrodes and the various methods to improve the capacitance and rate capability were introduced. In particular, the effect of pore length distribution (PLD) on kinetics of double-layer charging/discharging was discussed based upon the experimental and theoretical results in our work. And then we discussed in detail the applications of the activated carbon fibers to adsorbent materials for purification of liquid and gas.

Keywords: Activated carbon fiber, Activation method, Pore structure, Surface oxygen functional groups, Electric double-layer capacitor, Adsorbent.

1. Introduction

The activated carbon fibers have played a key role in many areas of modern science and technology such as storage of energy, purification of liquid and gas, separation of mixture and catalyst for reaction.[1-11] The advantages of the activated carbon fibers are the small diameter of the carbon fiber which minimises the diffusion limitation and allows rapid adsorption/desorption, uniform pore size distribution (PSD) and larger adsorption capacity at low concentration of adsorbates compared with conventional activated granular/powder carbons.

The porosity of the activated carbon fibers can be developed during the activation process, normally by gasification in steam and/or carbon dioxide.[12,13] The surface area and pore structure of the activated carbon fibers are greatly affected by degree of activation. During the activation process, various types of surface oxygen functional groups are formed on the pore surfaces of the activated carbon fibers.[12-14] The surface oxygen functional groups, *i.e.* chemical heterogeneities can be also effectively controlled by physical and chemical activation processes.

Although the porous structure of the activated carbon fibers mainly depends upon the activation agents and the activation conditions, the nature of the raw materials is the most important factor in determining the properties of resulting activated carbon fibers. The physicochemical properties of the activated carbon fibers such as pore structure and surface oxygen functional groups largely affect the adsorption capacity and electrochemical behaviour of the activated carbon fiber electrodes.

In this respect, this review provides a comprehensive survey of synthetic methods and physicochemical properties of the activated carbon fibers. Furthermore, as electrochemical applications of the activated carbon fibers to electrode materials for EDLC, the current issues in the improvement of electrochemical performance of the activated carbon fiber electrodes were discussed, along with our recent work.[15] And then we discussed in detail the applications of the activated carbon fibers to adsorbent materials for purification of liquid and gas.

2. Synthesis of the Activated Carbon Fibers

The common precursors for the activated carbon fibers are cellulose, rayon, polyacrylonitrile (PAN), phenolic resin, pitch and polyacetylenes, *etc.*[13] In the early 1960's, rayon was a popular carbon fiber precursor and is presently used in the nose cap and nozzle of various aerospace vehicles including the space shuttle.

However, the carbon yield of rayon is very low (35 wt.%) and large quantities of carbon fibers are no longer routinely produced from rayon due to the requirement of the high-temperature stretching in order to produce the carbon fibers with excellent mechanical and thermal properties. In this respect, rayon-based fibers have been replaced by PAN and pitch fibers

†E-mail: sipyun@webmail.kaist.ac.kr

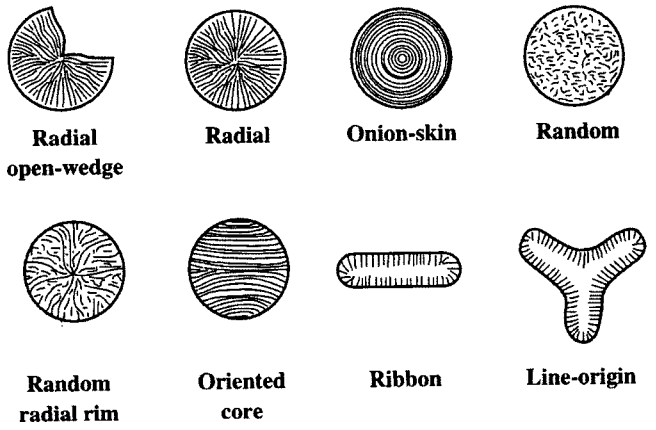

Fig. 1. Various textures of the mesophase pitch-based carbon fibers which can be developed by spinning the pitch fibers in different ways.

which are cheaper to produce the carbon fibers with high strength and modulus values. Currently, approximately 90% of all commercial carbon fibers are produced by using PAN and pitch as a carbonaceous precursor.

Fig. 1 illustrates the several possible textures of the mesophase pitch-based carbon fibers which can be developed by spinning the pitch fibers in different ways. The shape, texture, morphology and size of the carbon fibers may be controlled by changing the spinning conditions. Spinning involves the preparation of a precursor solution or melt, the extrusion of a precursor material through a die or spinnerette and the drawing of that material into a thin fiber. Commercial carbon fibers are produced by two different spinning techniques.[14]

The first of these, melt-spinning, involves the heating of thermoplastic material, such as Nylon, to temperatures above its melting point. A typical melt-spinning apparatus for PAN-based carbon fiber is shown in Fig. 2. In general, an extruder melts the precursor and pumps it into the spin pack. Then, the molten polymer is filtered before being extruded through a multi-holed spinnerette.

The filtered material is subjected to high extensional and shear stresses as it approaches and flows through the spinnerette capillaries. Finally, the fibers are drawn to generate axial orientation and are collected on a wind-up device. The crystallisation often occurs during fiber drawing. In the overall synthetic procedures of the carbon fiber, the spinning is followed immediately by a heat-treatment step in order to enhance the crystallinity of the carbon fiber and to alter the mechanical properties of the carbon fiber.

On the other hand, many precursor materials for the carbon fibers exhibit exceptionally high melting points, and thus the melt spinning is impractical for such materials. Fortunately, the solution spinning provides an alternative for these materials. The solution spinning includes two techniques: dry and wet spinning. In dry spinning, the polymer is dissolved in a volatile organic solvent. Hot air or inert gas is blown to the spin-line as it emerges from the spinnerette, which causes the volatile solvent to evaporate. The resultant fiber is wound much as in melt spinning.

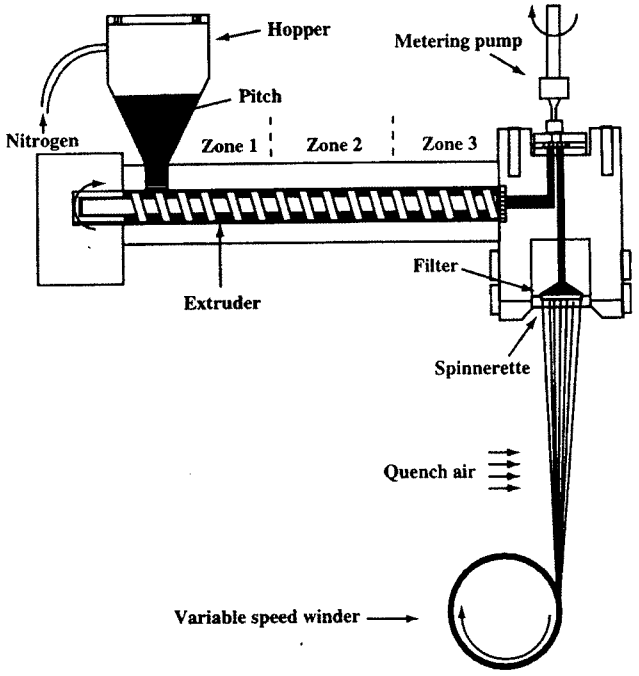

Fig. 2. Melt-spinning apparatus for pitch-based carbon fiber.

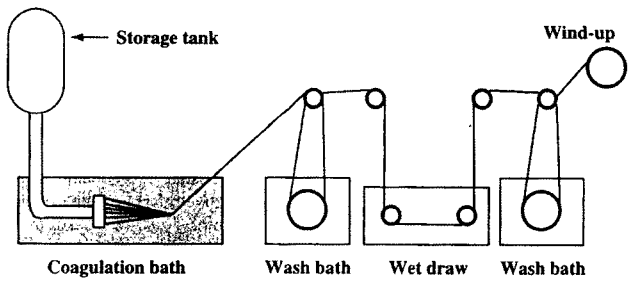

Fig. 3. Wet spinning apparatus for PAN-based carbon fiber.

If the precursor materials will neither melt nor dissolve in volatile solvents, the wet spinning can be used. Fig. 3 illustrates the wet spinning apparatus for PAN-based carbon fibers. Generally, PAN copolymer containing 93-95 wt.% acrylonitrile is dissolved in a solvent such as DMAc (dimethylacetamide) in order to form a highly concentrated polymer solution. The resulting solution is loaded in a storage tank and pumped into the wet spinning system.

In a manner similar to the melt spinning, the solution is filtered to minimize the presence of impurities and passed through the spinnerette. The fiber emerges through the small capillary holes of the spinnerette into a coagulation bath containing a fluid, such as ethylene glycol, which extracts the solvent from the fiber. The wet spinning is the most complicated spinning technique. Unfortunately, this technique is required for many carbon fiber precursors including PAN.

The carbon fibers are activated in order to possess high surface area and large pore volume.[15-22] The activated carbon fibers are generally prepared by following procedures: stabilisation, carbonisation and activation.[14] The first step in these processes involves a fiber oxidation, generally called stabili-

sation. The stabilisation process is essential for the quality of the resultant fibers since the spun fibers do not change their shape or structural properties during subsequent carbonisation.

The stabilisation is carried out in an oxidising atmosphere at temperatures in the range of 200°-300°C under tension in order to improve the mechanical properties without the shrinkage of the fiber. The heat treatment condition (temperature and time) for complete stabilisation depends upon the kind of gas, pressure, type of precursor and size of the fiber.

The stabilised fibers are further heat-treated in an inert atmosphere up to 1500°C (carbonisation). During the carbonisation process, a series of thermal reactions such as elimination of remaining hetero-atoms and polycondensation of aromatic units to larger carbon planes occur in the fiber axis. Subsequently, the carbonised fibers are activated in order to enlarge the volume and size of the pores which were already created during the carbonisation process and to create some new porosity. Most commonly employed activation methods are divided into physical and chemical activations.[23-34]

In physical activation, the gasification of the carbonised fiber usually occurs at higher temperature above 800°C in the presence of suitable oxidising gases such as steam, carbon dioxide CO_2, or a mixture of these. Activation of the carbon fiber in atmospheres of steam and CO_2 occurs by the following endothermic reactions.

$$C\,(s) + H_2O\,(g) \rightarrow CO\,(g) + H_2\,(g) \quad (1)$$

$$C\,(s) + CO_2\,(g) \rightarrow 2CO\,(g) \quad (2)$$

Since the reactions of the carbon with steam and CO_2 are both endothermic, the external heating is required to drive the above reactions and to maintain the reaction temperature. The activation with CO_2 involves a less energetic reaction than that with steam and thus requires a higher temperature.

The surface area, the pore size and the carbon yield of the activated carbon fibers are greatly influenced by oxidising gas, heat-treatment temperature and activation time. In addition, the oxidative activation introduced the surface acidic functional groups (SAFGs) on the pore surfaces of the carbon fibers. The amounts of the SAFGs can be also controlled by changing the activation conditions. Extensive burn-off at higher temperatures increases the surface area and pore size with less development of the SAFGs.

In chemical activation, the carbon fiber is impregnated with a chemical agent, and then the impregnated product is pyrolysed between 400° and 800°C in an inert atmosphere. After that, the pyrolysed product is cooled and washed exhaustively in order to remove the chemical agent, followed by filtration of the carbon materials. The chemical agents used are normally alkali, alkali earth metal, and some acids such as KOH,[19,26,27,32,33] K_2CO_3,[31] NaOH,[31,33] Na_2CO_3,[31] $ZnCl_2$,[17-20] and H_3PO_4,[20,30,32] *etc.*

The main advantages of the chemical activation compared to the physical activation are lower activation temperature, shorter activation time and higher development of the porosity. Furthermore, since the chemical agents used are just substances with dehydrogenation properties which inhibit formation of tar and reduce the production of other volatile products, the carbon yields of the chemically-activated carbon fibers are usually higher than those of the physically-activated carbon fibers. However, the general mechanism of the chemical activation is not well understood, as compared to that of the physical activation. Other disadvantages of the chemical activation are the need of additional washing procedure in order to remove the chemical agents and the corrosiveness of the chemical activation process.

Since the heat-treatment temperature used in the chemical activation is lower than that used in the physical activation, the porous structure is more developed in the case of the chemical activation. The higher the degree of impregnation, the larger is the pore size of the activated carbon fibers. Generally, kind of chemical agent, impregnation ratio of chemical agent to the carbonaceous material, and physical mixing method for distribution of chemical agent into the carbonaceous material largely affect the resulting pore structures of the chemically-activated carbon fibers.

3. Characterisation of Physicochemical Properties of the Activated Carbon Fibers

Following the International Union of Pure and Applied Chemistry (IUPAC) recommendations,[35] the pores are classified into three groups according to their size: (i) Pores with width (distance between the walls of a slit-shaped pore) smaller than 2 nm are called micropores, (ii) Pores with width between 2 nm and 50 nm are called mesopores, and (iii) Pores with width larger than 50 nm are called macropores.

Many researchers have attempted to characterise the porous structure of the activated carbons using nitrogen gas adsorption,[36-38] molecular probe [39,40] and small angle X-ray scattering.[41-43] Recently the porous structure of the activated carbon has been directly imaged using scanning tunneling microscopy (STM),[44] scanning electron microscopy (SEM) [45] and transmission electron microscopy (TEM).[46,47]

Fig. 4 illustrates comparative schematic pore structures of the activated carbon fiber and the activated carbon powder.[14] The pores of the activated carbon fibers open directly to the outer surface perpendicular to the fiber axis with minimum diffusion restriction due to the small diameter of the carbon fiber (10-20 μm). In contrast, for the carbon powder, the oxi-

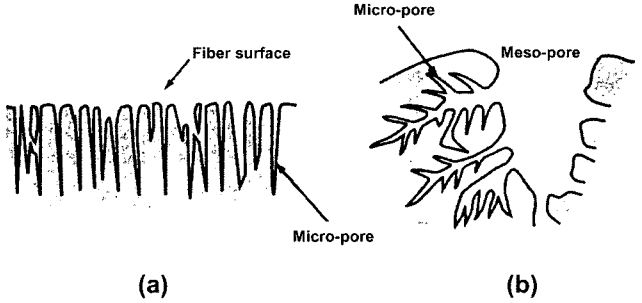

Fig. 4. Schematic representation of pore models of (a) activated carbon fiber and (b) activated carbon powder.[14]

dation starts at the outer surface and gradually proceeds to the interior of the powder. Therefore, the outer surfaces of the powder are more extensively oxidised to create the macropores of larger entrance diameters. Consequently, the outer zone and the core zone of the activated carbon powder have almost mesopores and micropores, respectively.

Lu and Zheng[48] reported that PAN-based activated carbon fibers have an open-celled structure with continuous porous network. They suggested that the pores of the activated carbon fiber are ellipsoidal in shape as proposed by Stoekli[49] from the analyses of the TEM images. Daley *et al.*[44] also reported that the porous structure of the phenol-based activated carbon fiber is stable and homogeneous from the STM observation. The micropores are ellipsoidal in shape and the pores are uniformly distributed throughout the bulk of the activated carbon fiber.

Oshida *et al.*[46] showed the TEM image of the cross section of the activated carbon fiber cut by a microtome. From the result that the pores comprising the activated carbon fibers are uniformly distributed without difference between the centre and periphery of the cross section, they suggested that the isotropic cross-sectional structure might result from the shear associated with melt spinning of the original fiber precursor.

The pore surfaces of the activated carbon fibers are composed of randomly distributed basal and edge planes. The basal plane is flat on the atomic scale, whereas the edge planes are heterogeneously composed of many of defects or oxygen functional groups attached on those planes.[13,14]

Fig. 5 depicts the schematic surface oxides which are formed on the pore surfaces of the activated carbon fibers. The PAN-based activated carbon fiber possesses a significant amount of nitrogen atoms varying from 3-10 wt.% dependent upon extent of activation. Cellulose- and phenol resin-based activated carbon fibers are non-graphitisable, and hence carry more oxygen functional groups. On the other hand, the pitch-based activated carbon fiber is more graphitic, and thus has least oxygen functional groups.

The irreversible physical adsorption of oxygen on carbon surfaces starts at ca. -40°C with the formation of surface oxides. The concentration of the oxygen functional groups

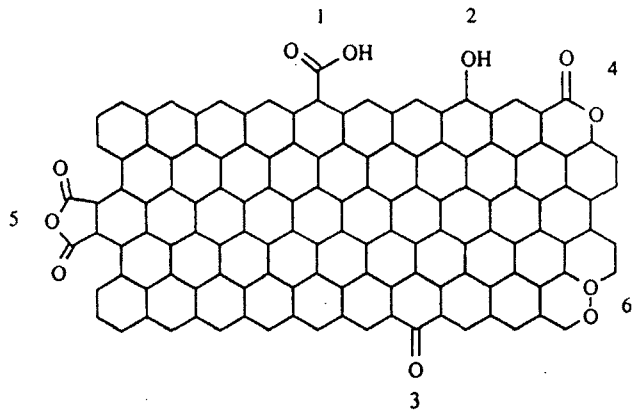

Fig. 5. Various types of surface oxygen functional groups formed on the activated carbon fiber: 1. carboxyl; 2. phenol; 3. quinon; 4. lactone; 5. carboxyl anhydride; 6. cycle peroxide groups.[13]

increases with an increase in the oxidation temperature and reaches a maximum at 400° to 500°C.[50] At higher temperatures, the oxygen functional groups are thermally unstable and hence decompose to CO and CO_2 gases.[51]

Three types of surface oxides (acidic, basic and neutral) have been generally known. Acidic surface oxides are formed when the carbon is treated with oxygen at temperatures near its ignition point or with an oxidising solution at room temperature. Several types of acidic surface oxides start to decompose under vacuum at ca. 250°C. Basic surface oxides are formed when a carbon surface is freed from all surface compounds by heating in a vacuum or in an inert atmosphere and comes into contact with oxygen only after cooling to low temperature.[52]

The pyrolysis of basic surface oxides reveals that each basic surface site contains two differently bound oxygen atoms; one is volatilised as CO and CO_2 at 900°C and the other is volatilised between 900° and 1200°C. Finally, the neutral surface oxides are formed by the irreversible adsorption of oxygen at unsaturated sites (>C=C<) on the carbon surface. The neutral surface oxides are more stable than the acidic surface oxides and they begin to decompose in the temperature range of 500° – 600°C.

4. Applications of the Activated Carbon Fibers

4.1. Electrode Materials for Electric Double-Layer Capacitor

Over the last two decades, the EDLCs have been considered as one of the most attractive energy storage devices because of their high power density, high capacitance, and high charging/discharging rates.[53-57] The highly porous carbons are widely used as the electrode materials in EDLCs, due to such advantageous features as high surface area, good electrical conductivity, and adequate corrosion resistance. Among those porous carbons, the activated carbon fibers have attracted considerable attention due to their high specific capacitance and uniform pore size distribution.

Momma *et al.*[54] investigated the effect of the electrochemical oxidation of the activated carbon fiber electrode on the double-layer capacitance by using a cyclic voltammetry and ac-impedance spectroscopy. In their work, it was elucidated that the electrochemical oxidation is effective for the enhancement of the double-layer capacitance due to the increases in the surface area and the amount of the SAFG. However, the inner resistance of the carbon electrodes increased by electrochemical oxidation.

Hsieh *et al.*[58] also studied the influence of oxygen treatment on the double-layer capacitance of the activated carbon fiber electrodes. In their work, 25% capacitance increase (e.g., from 120 to 150 F g^{-1} at a current density of 0.5 mA cm^{-2}) was achieved by thermal treatment of PAN-based activated carbon fiber at 250°C under an oxygen atmosphere for 6 h.

Ishikawa *et al.*[53] explored the effect of cold plasma treatment of activated carbon fiber cloth electrode (ACFCE) on electrochemical performance of EDLCs. The treatment with cold plasma which is performed in argon-oxygen atmosphere

at low temperature has been generally used as a novel method for the modification of the physical and chemical properties of carbon materials.[59-61] From their work, it was revealed that the amount of the micropores and the concentration of the SAFGs increased by cold plasma treatment.

They suggested that the increase in the amount of micropores obviously contributes to the increase in the double-layer capacitance, whereas the SAFGs attached on the carbon surface cause the self-discharging, *i.e.* current leakage. It was also reported from our laboratory[21] that the SAFGs impede the ion penetration into the pores during double-layer charging/discharging, and hence the more the amount of the SAFGs on the carbon electrode, the lower exhibits the rate capability. The negative effect induced by larger amount of the SAFGs and the positive effect derived from the increase in the microporosity may be compatible in the case of the carbon electrodes treated with cold plasma.

Recently, the size of the EDLC becomes an important problem for use in portable electric devices, but one of weak points of the activated carbon fiber is its low bulk density which makes the capacitor large in size and volume. Under these circumstances, Nakagawa *et al.*[56] prepared the activated carbon fiber with high bulk density (HD-ACF) without any binders using 'hot briquetting method'[62] in order to improve the bulk density of the activated carbon fiber. The capacitance per unit volume of the HD-ACF electrode was five times greater in value than that of the general activated carbon fiber electrode. Furthermore, the thickness of the HD-ACF electrode increased without change of the capacitance per unit weight of the electrode.

Much of the electro-active surface of the activated carbon fiber electrode is accessible only through the cumulative resistance of the electrolyte inside the pore. Therefore, the porous structure of the activated carbon fiber electrodes becomes one of the most important factors for the high double-layer charging/discharging rates. The pore structures of the activated carbon fiber electrode are closely related to both the electro-active surface area which enhances the capacity and the RC time constant distribution, the standard deviation of which reduces the rate capability in practical viewpoint.

It has been reported[54] that the activated carbon fiber electrode significantly deviated from the ideal impedance behaviour of a cylindrical pore in the impedance spectrum; nevertheless, it is well known that it exhibits quite narrow PSD. In recent years it has been demonstrated by many researchers[15,63-65] that the frequency dispersion or capacitance dispersion is intimately related to PSD or PLD.

Recently, in our laboratory,[15] the effect of PLD on kinetics of double-layer charging/discharging of the ACFCE was investigated in a 30 wt% H_2SO_4 solution using nitrogen gas adsorption, ac-impedance spectroscopy, current transient technique and cyclic voltammetry. The ac-impedance spectra, current transient and cyclic voltammograms are theoretically calculated as a function of standard deviation of PLD based upon the modified transmission line model (TLM).

The model to describe the electrochemical behaviour of the porous electrode was first treated by De Levie.[66-68] He represented a pore surface by a transmission line as shown in Fig. 6, and derived the following expression for the impedance of the pore, Z_o

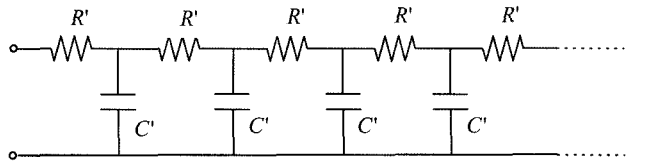

Fig. 6. Equivalent circuit of a transmission line network representing the ion migration into the pores. *R'* and *C'* denote the resistance of the electrolyte inside a pore and the double-layer capacitance of the electrode/electrolyte interface, respectively, both of which are taken per unit length.

$$Z_o = (1-j)\left(\frac{R'}{2\omega C'}\right)^{1/2} \coth\left[(1+j)\left(\frac{\omega R'C'}{2}\right)^{1/2} l_p\right] \tag{3}$$

with

$$R' = \frac{1}{k_e \pi r^2} \text{ and } C' = C_d 2\pi r \tag{4}$$

where R' is the resistance of the electrolyte inside a pore per unit pore length; C', the double-layer capacitance of the electrode/electrolyte interface per unit pore length; ω, angular frequency; l_p, the pore length; r, the pore radius; k_e, the conductivity of the electrolyte, and C_d represents the specific double-layer capacitance per unit area.

Considering PSD or PLD, the total impedance of the pores, Z_{tot} is given by

$$\frac{1}{Z_{tot}} = \int_{-\infty}^{\infty} \frac{1}{Z_o} f(x)dx \approx \sum_i \frac{1}{Z_{o,i}} f_i \Delta x_i \equiv \sum_i \frac{1}{Z_{o,i}} n_i \tag{5}$$

where $f(x)$ and $f(x)dx$ represent a distribution density function of PSD or PLD and the number of the pores between x and $x+dx$, respectively.

Song *et al.*[63,64] theoretically calculated the impedance spectra based upon Eq. (5) with such distribution functions of PSD as normal, lognormal, Lorentzian, log Lorentzian distributions. They concluded that the impedance spectra simulated based upon the TLM with different PSD functions share a common point that the wider PSD leads to the more frequency dispersion in the impedance spectra.

We assumed that the pore length l_p takes a lognormal distribution $f(x')$ as follows[15]

$$f(x') = \frac{V_{tot}}{\pi r^2 l_p} \frac{1}{\sqrt{2\pi}\sigma} \exp\left[-\frac{1}{2}\left(\frac{x'-\mu}{\sigma}\right)^2\right] \tag{6}$$

with

$$x' = \ln(l_p/l_o) \tag{7}$$

where x' denotes the natural logarithm of l_p divided by an arbitrary unit pore length l_o to obtain a dimensionless quantity; V_{tot}, the total pore volume; μ and σ are the mean value and the standard deviation of the distribution variable x', respectively.

Substituting $y=(x'-\mu)/\sigma$ into Eq. (6), we get

$$f(y) = \frac{V_{tot}}{\pi r^2 l_p}\frac{1}{\sqrt{2\pi}}\exp\left(-\frac{1}{2}y^2\right) \quad (8)$$

Hence, the Z_{tot} leads to

$$\frac{1}{Z_{tot}} = \int_{-\infty}^{\infty}\frac{1}{Z_o}f(y)dy = \int_{-\infty}^{\infty}\frac{1}{Z_o}\frac{V_{tot}}{\pi r^2 l_p}\frac{1}{\sqrt{2\pi}}\exp\left(-\frac{1}{2}y^2\right)dy \quad (9)$$

with

$$\int_{-\infty}^{\infty}\frac{1}{\sqrt{2\pi}}\exp\left(-\frac{1}{2}y^2\right)dy = 1 \quad (10)$$

From the quantitative coincidence of the impedance spectrum experimentally measured with that theoretically calculated with Eq. (9) as depicted in Fig. 7, we suggested that such non-ideal impedance behaviour of the ACFCE is mainly due to PLD, rather than due to PSD.

When PLD is considered together with the solution resistance R_{sol}, between reference electrode (R.E.) and working electrode (W.E.), the total current $I_{tot}(t)$ is written as[69]

$$I_{tot}(t) = \int I(t)f(y)dy$$

$$= \int\frac{2\Delta E}{R_{sol}}\sum_{n=1}^{\infty}\frac{\Lambda}{\Lambda^2+\Lambda+m_n^2}\exp\left(\frac{-m_n^2 k_e r t}{2C_d l_p^2}\right)\frac{V_{tot}}{\pi r^2 l_p}\frac{1}{\sqrt{2\pi}}\exp\left(-\frac{1}{2}y^2\right)dy \quad (11)$$

with

$$\Lambda = \frac{R_p}{R_{sol}} \text{ and } R_{sol} = \frac{l_s}{k_e \pi r^2} \quad (12)$$

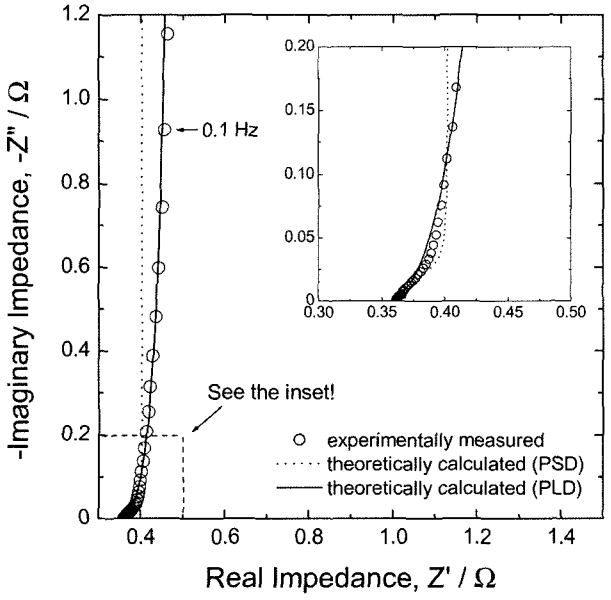

Fig. 7. Nyquist plot of the impedance spectrum experimentally measured on the activated carbon fiber cloth electrode (ACFCE) at an applied potential of 0.1 V (vs. SCE) in a 30 wt% H_2SO_4 solution. Dotted and solid lines represent the impedance spectra theoretically calculated based upon the transmission line model (TLM) in consideration of pore size distribution (PSD) and pore length distribution (PLD), respectively.[15]

where ΔE is the potential step; R_p, the resistance of the electrolyte inside a pore; l_s, the distance between R.E. and W.E.; m_n, the nth positive root of $(m \tan m - \Lambda)=0$; $f(y)$ and $f(y)dy$ represent a distribution density function of the pore length and the number of the pores between y and $y+dy$, respectively.

We theoretically calculated the cathodic current transients based upon the TLM as a function of σ of PLD. Fig. 8(a) and (b) illustrate the logarithmic cathodic current transients and the derivatives of the logarithmic cathodic current transients calculated from Eq. (11) with the change of σ of PLD, respectively. It is noted that as σ increases, the current decays more rapidly with time due to the dominant contribution of

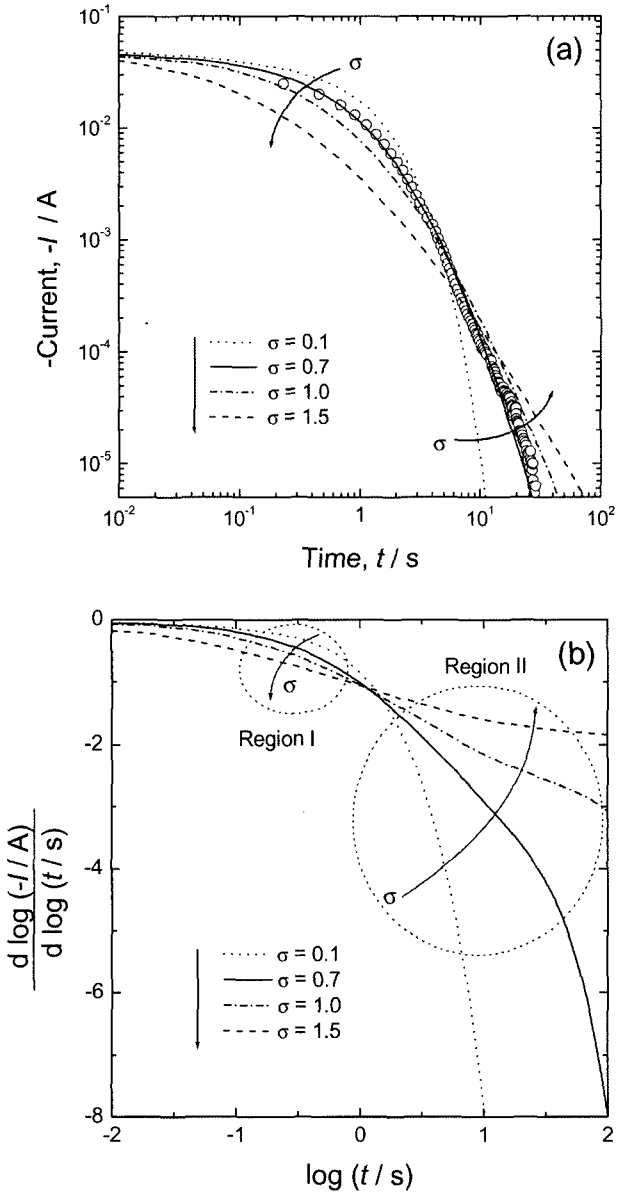

Fig. 8. (a) The cathodic current transients on a logarithmic scale and (b) the derivatives of the logarithmic cathodic current transients theoretically calculated from Eq. (11) based upon the TLM as a function of standard deviation σ of PLD. Open circles represent the cathodic current transient experimentally measured on the ACFCE.[15]

the pores with smaller length in the region I, whereas the current decays more slowly with time due to the dominant contribution of the pores with larger length in the region II.

In the case of potential scanning with a scan rate v, in consideration of PLD, the total current $I_{tot}(t)$ is given by[70]

$$I_{tot}(t) = \int I(t)f(y)dy$$
$$= \int(\beta_1 - \beta_2)vC_d 2\pi r l_p \frac{V_{tot}}{\pi r^2 l_p}\frac{1}{\sqrt{2\pi}}\exp\left(-\frac{1}{2}y^2\right)dy \quad (13)$$

with

$$\beta_1 = 1 - \sum_{n=1}^{\infty}\frac{2\Lambda^2}{m_n^2[\Lambda^2 + \Lambda + m_n^2]}\exp\left(\frac{-m_n^2 k_e rt}{2C_d l_p^2}\right) \quad (14)$$

$$\beta_2 = \sum_{n=1}^{\infty}\left(\frac{\Lambda^2 + m_n^2}{\Lambda^2 + \Lambda + m_n^2}\right)\exp\left(\frac{-m_n^2 k_e rt}{2C_d l_p^2}\right)\left(\frac{2}{m_n^2}\right)\sin^2 m_n \quad (15)$$

The rate capability γ_{cap} defined as the quotient of the reduced charge for the ACFCE divided by the reduced charge for the ideal double layer capacitor decreased with increasing σ of PLD, as shown in Fig. 9. Consequently, from the above theoretical and experimental results, it is concluded that the ion penetration into the pores during double-layer charging/discharging is more impeded as σ of PLD increases.

4.2. Adsorbent Materials for Purification of Liquid and Gas

The activated carbon fibers exhibit high specific surface area, highly permeable structure and very fast adsorption/desorption rates in gas and liquid filtration.[4,5,7,9,11,25,48,71-76] In this regard, the porous activated carbon fibers have attracted much attention as a low-cost adsorbent material for demineralisation (desalting) of solution and cleaning of the atmosphere.

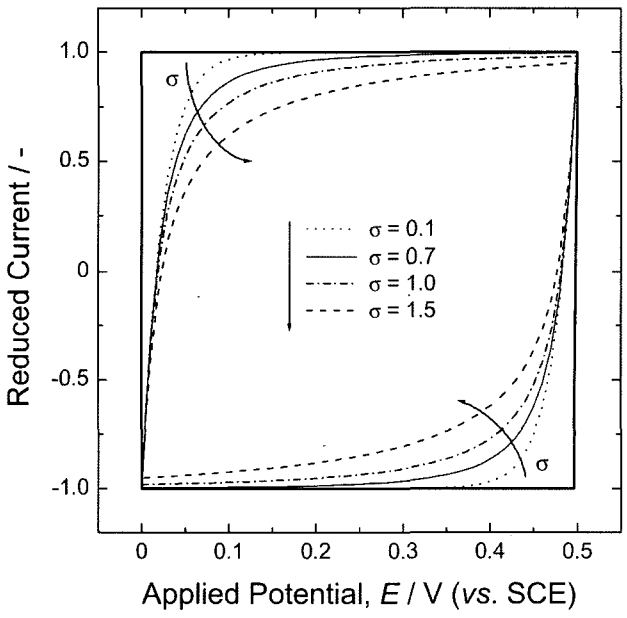

Fig. 9. Plots of the reduced current against the applied potential theoretically calculated based upon the TLM as a function of standard deviation σ of PLD at a scan rate of 20 mV s^{-1}. Solid bold line denotes the ideal double-layer capacitor where the time constant is zero.[15]

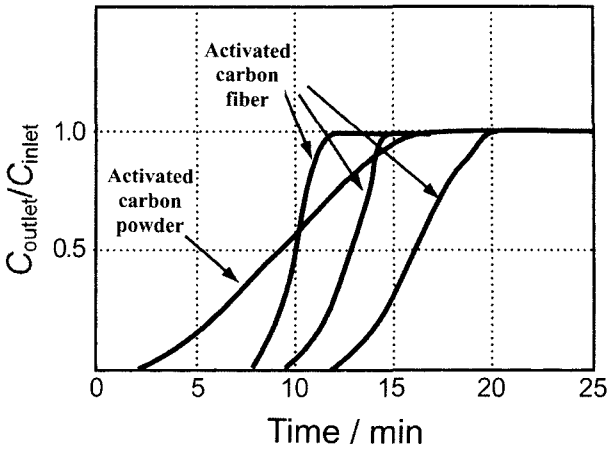

Fig. 10. The adsorption of benzene in a flow reactor over pitch-based activated carbon fibers and activated carbon powder.[14]

Fig. 10 illustrates the adsorption of benzene in a flow reactor over pitch-based activated carbon fibers and activated carbon powder.[14] The ratio of the benzene concentration of outlet to that concentration of inlet (C_{outlet}/C_{inlet}) shows an abrupt increase for the activated carbon fibers. Such rapid adsorption/desorption characteristics of the activated carbon fibers are ascribed to the shallow pores which open directly to the outer surface perpendicular to the fiber axis with minimum diffusion restriction, as previously shown in Fig. 4.

The porous structures of the activated carbon fibers are favourable for excellent capacity to effectively remove a large fraction of metal ions from dilute solution by electrodeposition. Demineralisation of dilute saline solutions requires the use of the porous carbon electrode with high specific surface area, since the capacity of the electrode in removing the ionic species from solution is dependent upon the electro-active surface area available for ion exchange[71,72] or ion adsorption[73,74]. It is reported[71] that the demineralisation involves weak acid oxygen groups on the carbon surface, as suggested by the following sequence of reactions:

$$H_2O + e^- \rightarrow H_{ads} + OH^- \quad (16)$$

$$-COOH + OH^- \rightarrow -COO^- + H_2O \quad (17)$$

$$-COO^- + Na^+ \rightarrow -COONa \quad (18)$$

When the activated carbon fiber electrode is cathodically polarised, a faradaic reaction occurs to produce adsorbed hydrogen and hydroxyl ions, which provide a suitable environment for the dissociation of acid groups, -COOH, on the carbon surface. The ionised acid group then reacts with Na^+ as given by Eq. (18). When the activated carbon fiber electrode is regenerated by anodic polarisation, the adsorbed hydrogen H_{ads} produced according to Eq. (16) is oxidised as follows

$$H_{ads} \rightarrow H^+ + e^- \quad (19)$$

and the pH is lowered so that proton exchange with Na^+ is favoured.

$$-COONa + H^+ \rightarrow -COOH + Na^+ \quad (20)$$

The carbon electrode oxidised by acid treatment exhibits a higher exchange capacity than untreated carbon electrode, since the oxidised carbon electrode exhibits a higher concentration of the SAFGs.

Now the use of the activated carbon fibers is extended to the removal of SO_2 from the atmosphere as well as from flue gas in order to solve the environmental problem such as an acid rain.[76] Kisamori *et al.*[75] reported that the basic principle of SO_2 removal is capture of SO_2 in the form of aqueous H_2SO_4. SO_2 is adsorbed, oxidised and hydrated into aqueous H_2SO_4 on the pore surfaces of the activated carbon fiber as follows

$$SO_2 \rightarrow SO_{2\ ad} \quad (21)$$

$$SO_{2\ ad} + 1/2O_2 \rightarrow SO_{3\ ad} \quad (22)$$

$$SO_{3\ ad} + H_2O \rightarrow H_2SO_{4\ ad} \quad (23)$$

The adsorbed H_2SO_4 should be recovered thermally in the form of SO_2 in order to regenerate the adsorption capacity of the activated carbon fiber.

The heat treatment of the activated carbon fiber before SO_2 adsorption increases the active sites for the oxidation of SO_2 due to the increase in the surface area. The larger the surface area of the activated carbon fiber, the larger exhibits the SO_2 adsorption capacity. On the other hand, the SAFGs on the activated carbon fiber should be removed by heat-treatment since they reduce the SO_2 adsorption capacity. So far, the role of the SAFGs in SO_2 adsorption is not clearly understood and the oxidising sites are now examined in order to reveal how they can oxidise SO_2 in the presence of O_2 and H_2O.

Acknowledgements

This work was supported by a grant from the Center for Advanced Materials Processing (CAMP) of the 21st Century Frontier R&D Program funded by the Ministry of Commerce, Industry and Energy (MOCIE), Republic of Korea. Furthermore, this work was partly supported by the Brain Korea 21 project.

Nomenclature

ACFCE	Activated carbon fiber cloth electrode
C_d	Specific double-layer capacitance per unit area
C'	Double-layer capacitance of the electrode/electrolyte interface per unit pore length
DMAc	Dimethylacetamide
ΔE	Potential step
EDLC	Electric double-layer capacitor
$f(x)$	Distribution density function of pore size distribution or pore length distribution
$f(x)dx$	Number of the pores between x and $x+dx$
γ_{cap}	Rate capability
HD-ACF	Activated carbon fiber with high bulk density
I	Current
I_{tot}	Total current
IUPAC	International union of pure and applied chemistry
k_e	Conductivity of the electrolyte
l_o	Arbitrary unit pore length
l_p	Pore length
l_s	Distance between reference electrode and working electrode
m_n	nth positive root of $(m \tan m - \Lambda)=0$
μ	Mean value of the distribution variables
v	Potential scan rate
PAN	Polyacrylonitrile
PLD	Pore length distribution
PSD	Pore size distribution
r	Pore radius
R'	Resistance of the electrolyte inside a pore per unit pore length
R_p	Resistance of the electrolyte inside a pore
R_{sol}	Solution resistance between reference electrode and working electrode
R.E.	Reference electrode
σ	Standard deviation of the distribution variables
SAFG	Surface acidic functional groups
SEM	Scanning electron microscopy
STM	Scanning tunneling microscopy
TEM	Transmission electron microscopy
TLM	Transmission line model
V_{tot}	Total pore volume
ω	Angular frequency
W.E.	Working electrode
x'	Natural logarithm of pore length l_p divided by an arbitrary unit pore length l_o to obtain a dimensionless quantity
Z_o	Impedance of the pore
Z_{tot}	Total impedance of the pores

References

1. I. Tanahashi, A. Yoshida, and A. Nishino, *J. Electrochem. Soc.*, **137(10)**, 3052 (1990).
2. A. Yoshida, I. Tanahashi, and A. Nishino, *Carbon*, **28(5)**, 611 (1990).
3. M. Endo, K. Takeuchi, Y. Sasuda, K. Matsubayashi, K. Oshida, and M.S. Dresselhaus, *Electron. Commun. Jpn.*, **77**, 98 (1994).
4. S. Kisamori, I. Mochida, and H. Fujitsu, *Langmuir*, **10**, 1241 (1994).
5. M. Suzuki, *Carbon*, **32(4)**, 577 (1994).
6. F. Stoeckli, T. A. Centeno, A. B. Fuertes, and J. Muñiz, *Carbon*, **34(10)**, 1201 (1996).
7. C. Brasquet and P. Le Cloirec, *Carbon*, **35(9)**, 1307 (1997).
8. Z. Li, M. Kruk, M. Jaroniec, and S.-K. Ryu, *J. Colloid Interface Sci.*, **204**, 151 (1998).
9. Z. Ryu, J. Zheng, and M. Wang, *Carbon*, **36(4)**, 427 (1998).
10. Y. V. Basova, H. Hatori, Y. Yamada, and K. Miyashita, *Electrochem. Commun.*, **1**, 540 (1999).
11. M. El-Merraoui, M. Aoshima, and K. Kaneko, *Langmuir*, **9**, 4300 (2000).
12. J. S. Mattson and H. B. Mark, Jr., "Activated Carbon: Surface

Chemistry and Adsorption from Solution", Marcel Dekker, New York (1971).
13. H. Marsh, E. A. Heintz, and F. Rodríguez-Reinoso, "Introduction to Carbon Technologies", Universidad De Alicante, Spain (1997).
14. H. Marsh and F. R. Reinoso, "Sciences of Carbon Materials", Universidad De Alicante, Spain (2000).
15. G.-J. Lee, S.-I. Pyun, and C.-H. Kim, *J. Solid State Electrochem.*, **8**, 110 (2004).
16. P. L. Walker, Jr., F. Rusinko, Jr., and E. Raats, *J. Phys. Chem.*, **59**, 245 (1955).
17. F. Caturla, M. Molina-Sabio, and F. Rodriguez-Reinso, *Carbon,* **29**, 999 (1991).
18. F. Rodríguez-Reinoso and M. Molina-Sabio, *Carbon*, **30**, 1111 (1992).
19. A. Ahmadpour and D. D. Do, *Carbon*, **34**, 471 (1996).
20. C. Namasivayam and K. Kadirvelu, *Bioresource Technol.*, **62**, 123 (1997).
21. C.-H. Kim, S.-I. Pyun, and H.-C. Shin, *J. Electrochem. Soc.,* **149**, A93 (2002).
22. S.-I. Pyun, C.-H. Kim, S.-W. Kim, and J.-H. Kim, *J. New Mat. Electrochem. Systems,* **5**, 289 (2002).
23. S. R. Tennison, *Applied Catalysis A: General*, **173**, 289 (1998).
24. C.-F. Chang, C.-Y. Chang, and W.-T. Tsai, *J. Colloid Interface Sci.*, **232**, 45 (2000).
25. Z. Ryu, J. Zheng, M. wang, and B. Zhang, *J. Colloid Interface Sci.*, **230**, 312 (2000).
26. H. Teng and S.-C. Wang, *Carbon*, **38**, 817 (2000).
27. D. Lozanó-Castelló, M. A. Lillo-Ródenas, D. Cazorla-Amorós, and A. Linares-Solano, *Carbon*, **39**, 741 (2001).
28. A. R. Sánchez, A. A. Elguézabal, and L. de La Torre-Saenz, *Carbon*, **39**, 1367 (2001).
29. F. Suárez-García, J. I. Paredes, A. Martínez-Alonso, and Juan M. D. Tascón, *J. Mater. Chem.*, **12**, 3213 (2002).
30. M. C. Baquero, L. Giraldo, J. C. Moreno, F. Suárez-García, A. Martínez-Alonso, and J. M. D. Tascón, *J. Anal. Appl. Pyrolysis*, **70**, 779 (2003).
31. K. Okada, N. Yamamoto, Y. Kameshima, and A. yasumori, *J. Colloid Interface Sci.*, **262**, 179 (2003).
32. A. M. Puziy, O. I. Poddubnaya, A. Martínez-Alonso, and F. Suárez-García, J. M. D. Tascón, *Carbon*, **41**, 1181 (2003).
33. J. A. Maciá-Agulló, B. C. Moore, D. Cazorla-Amorós, and A. Linares-Solano, *Carbon*, **42**, 1367 (2004).
34. F.-C. Wu, R.-L. Tseng, and R.-S. Juang, *J. Colloid Interface Sci.*, **283**, 49 (2005).
35. K. S. W. Sing, D. H. Everett, R. A. W. Haul, L. Moscou, R. A. Pierotti, J. Rouquérol, and T. Siemieniewska, *Pure Appl. Chem.*, **57**, 603 (1985).
36. E. M. Freeman, T. Siemienjewskam, H. Marsh, and B. Rand, *Carbon*, **8**, 7 (1970).
37. H. Marsh and B. Rand, *J. Colloid Interface Sci.*, **33(1)**, 116 (1970).
38. M. M. Dubinin and H. F. Stoeckli, *J. Colloid Interface Sci.*, **75(1)**, 34 (1980).
39. S. Kasaoka, Y. Sakata, E. Tanaka, and R. Naitoh, *International Chem. Eng.*, **29**, 101 (1989).
40. S. Kasaoka, Y. Sakata, E. Tanaka, and R. Naitoh, *International Chem. Eng.*, **29**, 734 (1989).
41. M. M. Dubinin. G. M. Plavnik. and E. D. Zaverina. *Carbon.* **2.** 261 (1964).
42. M. D. Foster and K. F. Jensen, *Carbon*, **29(2)**, 271 (1991).
43. P. W. Schmidt, *J. Appl. Cryst.*, **24**, 414 (1991).
44. M. A. Daley, D. Tandon, J. Economy and E. J. Hippo, *Carbon*, **34(10)**, 1191 (1996).
45. E. J. Roche, *J. Mat. Sci.*, **25**, 2149 (1990).
46. K. Oshida, K. Kogiso, K. Takeuchi, S. Kobayashi, M. Endo, M. S. Dresselhaus, and G. Dresselhaus, *J. Mater. Res.*, **5**, 2507 (1995).
47. M. Endo, T. Furuta, F. Minoura, C. Kim, K. Oshida, G. Dresselhaus,, and M. S. Dresselhaus, *Supramolecular Sci.*, **5**, 261 (1998).
48. A. H. Lu and J. T. Zheng, *J. Colloid Interface Sci.*, **236**, 369 (2001).
49. H. F. Stoekli, *Carbon,* **28**, 1 (1990).
50. H. W. Chang and S. K. Rhee, *Carbon*, **16**, 17 (1978).
51. K. Kinoshita, "Carbon: Electrochemical and Physicochemical Properties", John Wiley & Sons, New York (1988).
52. B. S. Weller and T. F. Young, *J. Am. Chem. Soc.*, **70**, 4155 (1948).
53. M. Ishikawa, A. Sakamoto, M. Morita, Y. Matsuda, and K. Isida, *J Power Sources*, **60**, 233 (1996).
54. T. Momma, X. Liu, T. Osaka, Y. Ushio, and Y. Sawada, *J Power Sources*, **60**, 249 (1996).
55. D. Qu and H. Shi, *J Power Sources*, **74**, 99 (1998).
56. H. Nakagawa, A. Shudo, and K. Miura, *J. Electrochem. Soc.*, **147**, 38 (2000).
57. T. C. Weng and H. Teng, *J. Electrochem. Soc.*, **148**, A368 (2001).
58. C.-T. Hsieh and H. Teng, *Carbon*, **40**, 667 (2002).
59. I. H. Loh, R. E. Cohen, and R. F. Baddour, *J. Mater. Sci.*, **22**, 2937 (1987).
60. C. Jones and E. Sammann, *Carbon*, **28**, 509 (1990).
61. C. Jones and E. Sammann, *Carbon*, **28**, 515 (1990).
62. K. Miura, H. Nakagawa, and H. Okamoto, *Carbon*, **38(1)**, 119 (2000).
63. H.-K. Song, Y.-H. Lee, and Le H. Dao, *Electrochim. Acta*, **44**, 3513 (1999).
64. H.-K. Song, H.-Y. Hwang, K.-H. Lee, and Le H. Dao, *Electrochim. Acta*, **45**, 2241 (2000).
65. G.-J. Lee and S.-I. Pyun, "Synthesis and Characterization of Nanoporous Carbon and Its Electrochemical Application to Electrode Material for Supercapacitor". In: C. G. Vayenas, B. E. Conway, R. E. White (eds) Modern Aspects of Electrochemistry, **No.40**, **Ch.8**, Kluwer Academic/Plenum Publishers, New York (2006) in press.
66. R. de Levie, *Electrochim. Acta*, **9**, 1231 (1964).
67. R. de Levie, *Electrochim. Acta*, **10**, 113 (1965).
68. R. de Levie, "Advances in Electrochemistry and Electrochemical Engineering", Ed. by P. Delahay, Vol. VI, John Wiley & Sons, New York (1967), p.329.
69. F. A. Posey and T. Morozumi, *J. Electrochem. Soc.*, **113**, 176 (1966).
70. L. G. Austin and E. G. Gagnon, *J. Electrochem. Soc.*, **120**, 251 (1973).
71. S. Evans and W. S. Hamilton, *J. Electrochem. Soc.*, **113**, 1314 (1966).
72. S. Evans, M. A. Accomazz, and J. E. Accomazzo, *J. Electrochem. Soc.*, **116**, 307 (1969).
73. A. M. Johnson and J. Newman, *J. Electrochem. Soc.*, **118**, 510 (1971).
74. Y. Oren and A. Soffer, *J. Electrochem. Soc.*, **125**, 869 (1978).
75. S. Kisamori, K. Kurod, S. Kawano, I. Mochida, Y. Matsummura, and M. Yoshikawa, *Energy & Fuels*, **8**, 1337 (1994).
76. I. Mochida, S. Kisamori, M. Hironaka, S. Kawano, Y. Matsumura, and M. Yoshikawa, *Energy & Fuels*, **8**, 1341 (1994).